Noise Radiated from an Edge in Turbulent Flow

David M. Chase*
Bolt Beranek and Newman Inc., Cambridge, Mass.

An evanescent-wave formulation relates sound radiated from subsonic turbulent flow at the edge of a semi-infinite rigid surface to a wavevector-frequency spectral density $P(K,\omega)$ of hydrodynamic pressure. This has been used to obtain the frequency spectra of nearfield pressure in the surface and of farfield radiated pressure and the cross-spectrum between them. A model differing from those used previously is suggested for $P(K,\omega)$ to fit the frequency dependence of nearfield (and radiated) pressure spectra measured in jet-flow experiments and is interpreted to indicate dominance by the mean-shear source term. Results are applied to a recent experiment where a jet streamed off a flat surface. With model parameters determined mainly from nearfield surface pressure spectra, the predicted radiated spectrum agrees well with that measured. The measured cross-correlations between nearfield and radiated pressure plotted vs edge distance from the nearfield point at different frequencies roughly coalesce when normalized in accord with a predicted universal form and agree adequately with the result of the model. Significant validation of the method and of the proposed characterization of hydrodynamic pressure is thus obtained for the given flow configuration. Extension to two-sided flows is discussed.

Nomenclature

c = sound velocity in ambient fluid
$C(x_0,\omega)$ = cross-coherence between farfield pressure and pressure on rigid surface at distance $-x_0$ from edge
c_ν = coefficient in model spectral density of hydrodynamic pressure Eq. (24)
D = diameter of jet orifice
$2h$ = L sec α, the length of flow-immersed edge
k_0 = ω/c
(k_1,k_3), $(\tilde{k}_1,\tilde{k}_3)$ = components of planar wavevector $\boldsymbol{K}$ along x, z, and $\tilde{x}$, $\tilde{z}$, respectively (see Fig. 1)
L = breadth of fluctuating flow over edge
$p^i(\boldsymbol{r})$ = incident (evanescent) pressure field
$p^s(\boldsymbol{r})$ = edge-scattered pressure field
$p(\boldsymbol{r})$ = total pressure field
$P(\boldsymbol{K},\omega)$ = wavevector-frequency spectral density of hydrodynamic pressure
$P(\omega)$ = frequency spectral density of point hydrodynamic pressure
$P(\boldsymbol{r},\omega)$ = frequency spectral density of pressure at $\boldsymbol{r}$
$\boldsymbol{r}$ = [= (x, y, z)] radius vector to field point from midpoint of flow-immersed edge
$\boldsymbol{R}$ = (x, z)
U_0 = exit velocity of jet
u = effective convection velocity, e.g., in Eq. (24)
v = dispersion velocity characterizing coherence of hydrodynamic pressure in convected frame, Eq. (24)
α = angle between mean velocity of fluid and normal to edge
Δ = scale characterizing broadband hydrodynamic pressure correlation (large-eddy scale)
θ, ϕ = polar coordinates of field point with edge as polar axis
μ = v/u
ν = exponent characterizing functional dependence in model for hydrodynamic pressure, Eq. (24)
σ = $\omega|x_0|/u$
τ_m = time delay associated with phase of cross-spectrum (see definition of C)
ω = radian frequency (= $2\pi f$)

Submitted June 7, 1974; presented as Paper 74-570 at the AIAA 7th Fluid and Plasma Dynamics Conference, Palo Alto, California, June 17-19, 1974; revision received January 17, 1975. This work was supported by Office of Naval Research, Acoustic Programs Branch, under Contract N00014-69-C-0264.

Index category: Aircraft Noise, Aerodynamics (including Sonic Boom).

*Senior Scientist, Underwater Acoustics Department, Physical Sciences Division.

I. Introduction

In fluctuating fluid flows, solid surfaces play a dual role: first, in determining the structure of the flow itself; and, second, in radiating noise as acoustic impedance discontinuities. Such discontinuities or inhomogeneities scatter fluctuations in the flowfield—which, for low Mach numbers, have predominantly high, nonradiating wavenumbers—into a radiated acoustic field. Significant contributions to total radiated spectra can derive from flow at the

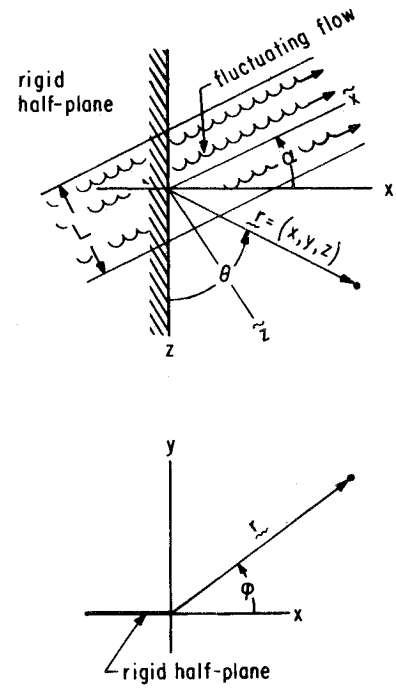

Fig. 1 Geometry for sound radiation by fluctuating flow across the edge of a rigid half-plane.

edges of thin members, such as airfoils, flaps, or control surfaces. Except sometimes within narrow frequency bands of structural resonances, these members (even in underwater applications) may usually be regarded as rigid.

In the limiting case where the surface dimensions, at given frequency, are small in comparison with the sound wavelength, the surface-related radiated sound pressure is of dipole character and proportional to the net fluctuating force on the surface. In the opposite limiting case, where the surface dimensions are large, the acoustic problem becomes one of edge diffraction. For this case, recent treatments[1,2] express the surface-related radiated sound in terms of an essentially hydrodynamic fluctuating pressure field defined on a surface, circumventing consideration of radiation by Lighthill volume sources in the presence of the edge.[3] These treatments are applicable, without further assumptions, to the instance where the turbulent flow is confined to one side. The two formulations of the acoustic problem are obtained by applying Green's theorem to the Lighthill-Curle equation at given frequency, first in the half-space opposite the flow, with the Green's function corresponding to presence of the rigid half plane, and, second, in the whole of space, with the Green's function corresponding to homogeneous fluid.

More explicitly, consider first the pressure radiated by a fluid flow within a volume V_0 contained within a larger volume V of fluid, where V is enclosed by a surface S that excludes but may contact solid bodies or other regions of inhomogeneous character.[4] Let $G(\mathbf{r}',\mathbf{r})$ denote a Green's function for the Helmholtz equation

$$(\nabla^2+\omega^2/c^2)G(\mathbf{r}',\mathbf{r})=-4\pi\delta(\mathbf{r}-\mathbf{r}')$$

that satisfies the outgoing wave condition at remote segments of S but is otherwise arbitrary. In a frequency-domain representation (with time factor $e^{-i\omega t}$ suppressed), for $\mathbf{r}$ outside V_0 the basic equation may be written as

$$4\pi p(\mathbf{r})=\int_V dV'\,T_{ij}\partial^2 G/\partial x_i'\partial x_j'$$

$$-\int_S dS'\,(\rho v_i v_n+p_i)\partial G/\partial x_i'+i\omega\int_S dS'\,\rho v_n G \qquad (1)$$

where the summation convention is used. Here p_i is the vector stress exerted by the fluid on the surface S, and v_n is the normal component of fluid velocity outward from V. Nominally, T_{ij} is the (frequency transform of the) Lighthill source tensor

$$T_{ij}=\rho v_i v_j+p_{ij}-c^2\rho\delta_{ij}$$

where v_i denotes fluid velocity and p_{ij} the stress tensor. For convergence, however, as emphasized in Ref. 5 (and implicit in the definition of V_0), the equations must be interpreted in terms of some meaningful approximation to T_{ij} that decreases sufficiently rapidly outside the region of primary fluctuating flow.

Now let the flow occur on one side of the rigid half-plane $y=0$, $x<0$. As in Ref. 1, apply Eq. (1) in the opposite half-space and choose G to be obtained byi maging, with opposite sign, the Green's function G_1 that satisfies $\partial G_1/\partial y=0$ for $y=\pm 0$, $x<0$. If the volume integral representing the spillover of Lighthill sources into the opposite half-space is neglected, Eq. (1) then yields

$$4\pi p(\mathbf{r})=-2\int_{S_+} dS'\,(p+\rho v_2^2)\partial G_1/\partial y' \qquad (2)$$

where S_+ denotes the half-plane extension $y=0$, $x>0$. The source term ρv_2^2 here is presumably negligible, since linear acoustics is applicable in the bounding source-free half-space. The required pressure p on S_+ is hydrodynamic, since the diffracted pressure from the rigid half-plane vanishes there.

For this same one-sided flow, now apply Eq. (1) instead in all space and choose G to be the homogeneous-space Green's function. The result is given by

$$4\pi p(\mathbf{r})=\int_{S_-} dS'\,(p_+-p_-)\partial G_0/\partial y'$$

$$+\int dV'\,T_{ij}\partial^2 G_0/\partial x_i'\partial x_j'$$

$$-\int_{S_-} dS' p_{\alpha+}\partial G_0/\partial x_\alpha' \qquad (3)$$

where $p_\pm$, $p_{\alpha+}$ ($\alpha=1$, 3 only) denote the pressure and shear stress exerted by the fluid on the upper (flow-bounding) (+) and lower (−) faces of the rigid half-plane, S_-. The formulation of edge-radiation in Ref. 2 may be regarded as based on Eq. (3), with omission of the volume integral, which does not involve the radiative effect of the edge, and neglect of the shear-stress contribution (see Ref. 2, Sec. 5).

In the latter formulation the pressure difference, p_+-p_-, across the rigid half-plane in Eq. (3) is obtained for each planar wavevector by expressing the solution to the problem of diffraction of an incident evanescent sound wave. (The wave is evanescent, since, in application to subsonic flow, its wavenumber exceeds that of sound.) This procedure rests on the irrelevance of the turbulent flow to the acoustic impedance of the fluid and the presumption that pressure and density variations at the rigid surface beneath the flow are related in the same way as outside the primary flow. The incident pressure wave, in the plane of the surface, may be identified with the hydrodynamic pressure wave of the first formulation. In Eqs. (2) and (3) the terms involving p and p_+-p_-, respectively (the only ones retained), then prove to yield the same result for the diffracted pressure field. Since, however, the second formulation provides the total pressure even on the flow-containing side of the surface, we employ it here.

A statistical description of the planar hydrodynamic pressure is needed, adequate at least within a few large-eddy scales of the edge. This pressure is modeled as locally streamwise-homogeneous. The corresponding wavevector-frequency spectral density is then to be based on a model thought appropriate for the turbulent flow upstream or downstream, without explicit concern for the hydrodynamic role of the edge, except in the determination of numerical parameters. The model need be valid only for wavevectors within the convective ridge, where the spectral density is high.

It might be hoped, by further development and validation of this approach, to parametrize the spectral density of a pertinent hydrodynamic pressure for more general flow configurations and estimate the effect of configuration changes on parameter values and, hence, on the radiated sound field. At the same time, this approach via gross modeling of the pressure field is not likely to be useful in constructing predictions for the edge tones or other narrowband contributions to radiated noise that have been found important under certain conditions, especially where the flow on one side of the surface remains laminar.[6-8]

In the rest of this paper, we first describe the rederivation by the second formulation of results previously obtained by the first and their extension to cross-spectra between near-field and radiated pressure. We then give results for a suggested explicit model form for hydrodynamic pressure modified and generalized from those previously applied. Finally, by these results, we analyze a recent jet-flow experiment well suited for assessment and development of this approach. We also comment on the instance of two-sided flow.

II. The Radiated Pressure Field and Related Spectra

The flow geometry considered is shown in Fig. 1. The rigid half-plane is defined by $y=0$, $x<0$. The fluctuating flow

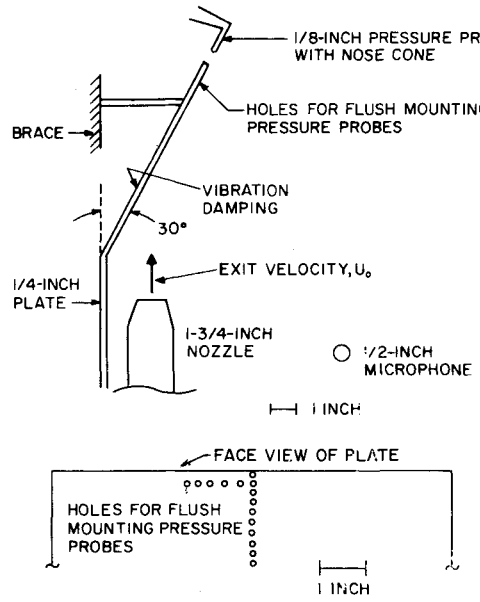

Fig. 2 Jet and plate test setup (Scharton, Pinkel, and Wilby[9]).

along the x-z plane on the $y<0$ side emerges at mean angle α relative to the edge-normal direction x. Results will be restricted to low Mach numbers.

The diffracted field corresponding to an evanescent incident field with definite wavenumber components parallel and normal to the edge was written by Chandiramani[2] from the available solution (usually applied to a propagating incident field) in the form of a single integral over a scattered wavenumber component (k_1') normal to the edge. The solution was obtained by the Weiner-Hopf or a related technique. Since, where the far field is in view, we wish rather to consider a flow of finite lateral extent, we must superpose incident waves having a distribution of wavenumber components k_3' parallel to the edge. This done, we may evaluate the pertinent wavevector integral for scattered pressure at points in the far field by the method of stationary phase [Eq. (11)]. At arbitrary field points, more generally, we may express the diffracted field for each fixed k_3' in terms of an integral over a closed contour in the complex k_1' plane, which is then the sum of a residue and a branch-cut integral. At points on the rigid surface in the nearfield limit, the result reduces to a pressure-doubling reflected wave decreased by a term proportional to a complementary error function of complex argument [Eq. (12)]. This yields a Fresnel type of oscillatory decrease of the scattered pressure from pressure-doubling equality with the incident wave far upstream to a vanishing value at the edge. We now develop these results somewhat more explicitly.

Let $\hat{p}(\boldsymbol{K},\omega)$ denote the Fourier amplitude for a realization of hydrodynamic pressure in the plane $y=0$. We accommodate the finite lateral extent of the flow by multiplying the resulting pressure field by an appropriate function, $g(2\bar{z}/L)$ say, whose exact form depends on the flow variation at the lateral edges and is of no present interest, but which, if normed so that $g(0)=1$, satisfies the condition that $g(\xi)<<1$ for $\xi\geq 1$. In the plane $y=0$, the unscattered evanescent pressure field is thus given by

$$p^i(x,z)=g(2\bar{z}/L)\int d^2\boldsymbol{K}e^{i\boldsymbol{K}\cdot\boldsymbol{R}}\hat{p}(\boldsymbol{K}) \tag{4}$$

where we suppress the time-dependent factor $e^{-i\omega t}$ and, when convenient, the argument ω. By introduction of the Fourier transform of $g(\xi)$, say $\hat{g}(\sigma)$, and the geometric relation $\bar{z}=z\cos\alpha+x\sin\alpha$, we may express p^i of Eq. (4) as a transform of convolved transforms.

To express the scattered pressure $p^s(\boldsymbol{r})$ in terms of the scattered wave of Eq. (23a) of Ref. 2, we have then only to form the wavevector superposition just specified. We obtain

$$p^s(\boldsymbol{r})=\int d^2\boldsymbol{K}\hat{p}(\boldsymbol{K})H^s(\boldsymbol{K},\boldsymbol{r}) \tag{5}$$

where

$$H^s(\boldsymbol{K},\boldsymbol{r})\equiv\int_{-\infty}^{\infty}dk_3'h\hat{g}[(k_3'-k_3)h]$$

$$\times C(k_1'',k_3',z)I(k_1'',k_3',x,y) \tag{6}$$

$$k_1''\equiv k_1+(k_3'-k_3)\tan\alpha \tag{7}$$

and, similarly to Eqs. (23b) and (23c) of Ref. 2,

$$C(k_1,k_3',z)\equiv i(2\pi)^{-1}[k_1+(k_0^2-k_3'^2)^{1/2}]^{1/2}e^{ik_3'z} \tag{8}$$

$$I(k_1,k_3',x,y)\equiv\int_{-\infty}^{\infty}dk_1'\exp i[k_1'x+(k_0^2-k_1'^2-k_3'^2)^{1/2}y]$$
$$\times(k_1'-k_1)^{-1}[(k_0^2-k_3'^2)^{1/2}+k_1']^{-1/2} \tag{9}$$

in which, as in Ref. 2, proper care must be given to phase definition.

In the far field limit where

$$\omega r/c>>1,\qquad r>>h \tag{10}$$

by the method of stationary phase, we obtain the following asymptotic form for H^s of Eq. (6)

$$H^s(\boldsymbol{K},\boldsymbol{r})\rightarrow -2^{1/2}(h/r)e^{ik_0r}(\sin\theta)^{1/2}\sin\tfrac{1}{2}\phi$$
$$\times k_0^{1/2}(k_1''+k_0\sin\theta)^{1/2}[k_1''-k_0\sin\theta\cos\phi]^{-1}$$
$$\times\hat{g}[(k_0\cos\theta-k_3)h] \tag{11}$$

where k_1'' is understood here as given by Eq. (7) with $k_3''\rightarrow k_0\cos\theta$(Fig. 1). The result (11) differs from that obtained by the method of Ref. 1, Eq. (14) [with $g(\xi)$ taken as 1 for $|\xi|<1$ and zero for $|\xi|>1$] by a factor that equals unity to order zero in k_0/k_1, i.e., the results agree at low Mach number.†

To evaluate the integral Eq. (9) for r in the nearfield, we consider for $x<0$ the corresponding integral over a closed contour in the lower half of the complex k_1' plane. This contour runs along the entire real axis, passing below the terminus, $k_d\equiv(k_0^2-k_3''^2)^{1/2}$, of the branch cut in the upper half-plane (Ref. 2, Fig. 2) but above the terminus $-k_d$ of that in the lower half-plane, and encompassing the pole at k_1''. The rest of the circuit consists of a semicircle (say) at infinity, opened at the lower branch-cut exit, together with a connecting path along both sides of the lower cut, which is thereby excluded from the domain enclosed. The branch point $-k_d$ lines on the negative real axis for $|k_3'|<k_0$ and on the negative imaginary axis for $|k_3'|>k_0$

We consider only points on the rigid surface ($x<0$, $y=0+$) in the nearfield limit where $\omega|x|/c<<1$ and the further limit where $\omega/c<<k_1''$, as suffices at low Mach number. The desired product CI in Eq. (6) is then found to reduce to

$$CI(y=0)\rightarrow\exp i(k_1''x+k_3'z)$$
$$\times\{1-\mathrm{Erfc}([(|k_3'|-ik_1'')|x|]^{1/2})\} \tag{12}$$

where the first term represents the residue at $k_1'=k_1''$ and the second the branch-cut integral. The incident pressure corresponding to the scattered pressure Eq. (12) is exp $[i(k_1''x+k_3'z)]$ (for $y=0$), so that the total pressure for $x<0$, $y=0+$

†In Ref. 1, the right member of Eq. (14) should be multiplied by a factor 2 on account of a mistaken factor ½ in the first term in Eq. (8). The difference by terms of higher order in k_0/k_1 might be expected in view of the approximation of Eq. (7) of Ref. 10.

is obtained by replacing 1 by 2 in the first term. In the extended half-plane ($x>0$, $y=0$), on the other hand, the scattered pressure vanishes. From Eqs. (5, 6, and 12), in the subject limit we have, with $p=p^i+p^s$,

$$p(x,0,z)\rightarrow \int d^2K\hat{p}(\boldsymbol{K}) \times \int_{-\infty}^{\infty} dk_3' h\hat{g}((k_3'-k_3)h)\exp i(k_1''x+k_3'z) \times \begin{cases} 1+\mathrm{Erf}\{[(|k_3'|-ik_1'')|x|]^{1/2}\} & \text{for } x\leq 0 \\ 1 & \text{for } x\geq 0 \end{cases} \quad (13)$$

with k_1'' still given by Eq. (7) and $|\arg(|k_3'|-ik_1'')^{1/2}|<\pi/2$. Since $\mathrm{Erf}(\xi)\rightarrow 1$ for $\xi\rightarrow\infty$, the upper form yields pressure-doubling, as it should, as $x\rightarrow -\infty$.

This approximate solution for pressure in the near and far fields is applicable to each realization of the incident field. Under the intended assumption of planar statistical homogeneity of the hydrodynamic (incident) pressure field, the expectation of products of pressure amplitudes may be expressed, as usual, in terms of its spectral density $P(\boldsymbol{K},\omega)$.

First, consider the frequency spectral density, $P(x,z,\omega)$, of total pressure on the rigid surface at points in the nearfield well removed from the lateral boundaries of flow on assumption that L greatly exceeds the pressure-coherence scale, i.e., $L>>(\delta\tilde{k}_3)^{-1}$, where $\delta\tilde{k}_3=(\omega^2/u^2+\Delta^{-2})^{1/2}$ measures the breadth in $\tilde{k}_3$ of the mean-convective ridge of $P(\boldsymbol{K},\omega)$; e.g., see Eq. (24). Then we have $h\hat{g}[(k_3'-k_3]\rightarrow\delta(k_3'-k_3)$ in Eq. (13) and obtain, independently of α and z,

$$P(x,z,\omega)\rightarrow\int d^2K P(\boldsymbol{K},\omega) \times \begin{cases} |1+\mathrm{Erf}\{[(|k_3|-ik_1)|x|]^{1/2}\}|^2 & x\leq 0 \\ 1 & x\geq 0 \end{cases} \quad (14)$$

The integrand in Eq. (14) for the spectrum at a fixed nearfield position on the rigid surface oscillates with the streamwise wavevector component k_1 but, with increasing lateral component k_3, tends more rapidly toward the pressure-doubling limit as the pressure oscillations along the edge increasingly average out.

Next, consider the spectral density, $P(\boldsymbol{r},\omega)$, of pressure in the farfield as obtained from Eqs. (5) and (11). For $L>>\Delta$, we have

$$\int_{-\infty}^{\infty} d\sigma|\hat{g}(\sigma)|^2=(2\pi)^{-1}\int_{-\infty}^{\infty} d\xi|g(\xi)|^2\simeq\pi^{-1}$$

We set $P(\boldsymbol{K},\omega)\equiv P(\tilde{k}_1,\tilde{k}_3,\omega)$, where $\tilde{k}_1$ is streamwise (Fig. 1); the mean-convective peak of this function at $\tilde{k}_1\simeq\omega/u$ has width $\delta\tilde{k}_1\sim(v/u)\delta\tilde{k}_3$, where v is of the order of the rms turbulence velocity [e.g., see Ref. 1, Eq. (23)]. On assumption that $\omega\Delta/u>>v/u$ (so that the peak in $\tilde{k}_1$ is sharp: $u\delta\tilde{k}_1/\omega<<1$) and $u/c<<1$, we derive from Eqs. (5) and (11), just as previously in Ref. 1 (p. 1016)

$$P(\boldsymbol{r},\omega)\simeq\pi^{-1}(u/c)Lr^{-2}\sec\alpha\sin\theta\sin^2\tfrac{1}{2}\phi \times\int d\tilde{k}_1 P(\tilde{k}_1,\tilde{k}_1\tan\alpha,\omega) \quad (15)$$

For $\tan\alpha<<(v/u)^{-1}$ (i.e., at flow angles not too nearly tangential, so that pressure decorrelation along the edge is due mainly to the transverse, not the streamwise, component), Eq. (15) is approximated by

$$P(\boldsymbol{r},\omega)\simeq\pi^{-1}(u/c)Lr^{-2}\sec\alpha\sin\theta\sin^2\tfrac{1}{2}\phi \times M(0,[\omega/u]\tan\alpha,\omega] \quad (16)$$

where, more generally,

$$M(\zeta_1,\tilde{k}_3,\omega)\equiv\int_{-\infty}^{\infty} d\tilde{k}_1\exp i\tilde{k}_1\zeta_1 P(\tilde{k}_1,\tilde{k}_3,\omega) \quad (17)$$

For normal incidence ($\alpha=0$), in particular, the farfield pressure spectrum in approximation (16) is thus proportional to the streamwise-wavenumber integral of the wavevector spectral density of hydrodynamic pressure at zero transverse wavenumber or, equivalently, to the integral of the cross-spectral density of point hydrodynamic pressure over transverse separations at zero streamwise separation, i.e., to the product of the point spectrum and the (frequency-dependent) transverse scale. The farfield spectrum has the characteristic angular dependence for knife-edge diffraction and is proportional to Mach number to one lower power than that for dipole radiation from flow over a small surface.

Finally, consider the cross-spectral density, $P(\boldsymbol{r},\boldsymbol{R}_0,\omega)$, between the radiated farfield pressure at $\boldsymbol{r}$ and the nearfield pressure at $\boldsymbol{R}_0=(x_0<0,0,z_0)$ on the rigid surface, as obtained from Eqs. (5, 11, and 13). Consideration is restricted in this instance, for simplicity, to $\alpha=0$. Under the previously cited conditions

$$\omega r/c>>1, r>>L,\ u/c<<1,\ \omega\Delta/u>>v/u$$

$$(\omega^2/u^2+\Delta^{-2})^{1/2}L>>1,\ \omega|x_0|/c<<1$$

and the further condition

$$(|x_0|/L)(\omega L/u)^{-1}<<1$$

we obtain, by approximations similar to those leading to Eqs. (14 and 16),

$$P(\boldsymbol{r},\boldsymbol{R}_0\omega)\simeq-(2u/c)^{1/2}(\sin\theta)^{1/2}\sin\tfrac{1}{2}\phi \times r^{-1}\exp -i(\omega/c)(r-z_0\cos\theta)\ \tilde{M}(x_0,\omega) \quad (18)$$

where

$$\tilde{M}(x_0,\omega)\equiv\int dk_1 e^{ik_1x_0}P(k_1,0,\omega) \times\{1+\mathrm{Erf}[(-ik_1|x_0|)^{1/2}]\} \quad (19)$$

The result is thus proportional to the sum of the cross-spectral density of hydrodynamic pressure for streamwise separation equal to the distance of the nearfield point from the edge (at vanishing lateral wavenumber) and a second term due to the acoustic wave diffracted upstream. For the cross-spectrum with the purely hydrodynamic pressure where $x_0>0$ (without conditions on $|x_0|$), the factor $\tilde{M}$ in Eq. (18) is replaced by $M(x_0,\omega)$, where

$$M(x_0,\omega)\equiv\int dk_1 e^{ik_1x_0}P(k_1,0,\omega) \quad (20)$$

[$\equiv M(x_0,0,\omega)$ of Eq. (17)]. The normalized cross-spectrum P_N with magnitude (cross-coherence) C and phase $\omega\tau_m-\pi$, say, is formed as

$$P_N(\boldsymbol{r},\boldsymbol{R}_0,\omega)\equiv -Ce^{i\omega\tau_m} =P(\boldsymbol{r},\boldsymbol{R}_0,\omega)/[P(\boldsymbol{R}_0,\omega)P(\boldsymbol{r},\omega)]^{1/2} \quad (21)$$

By Eqs. (15, 18, and 21) we may then write

$$C=(2\pi)^{1/2}\tilde{M}(x_0,\omega)/[P(x_0,\omega)M(0,\omega)L]^{1/2} \quad (22)$$

$$\tau_m=c^{-1}(r-z_0\cos\theta)-\omega^{-1}\arg\tilde{M}(x_0,\omega) \quad (23)$$

where $P(x_0, \omega)$ denotes $P(x_0, z_0, \omega)$ as given (independent of z_0) by Eq. (14), and $\tilde{M}$ is to be replaced by M when $x_0 > 0$.

III. Model for Hydrodynamic Pressure and Resulting Spectra

We now introduce a more explicit model form for the hydrodynamic pressure spectrum, $P(\mathbf{K}, \omega)$

$$P(\mathbf{K}, \omega) = c_\nu \rho^2 v^3 \Delta^{-2(\nu-2)} k_1^2 K_*^{-2\nu-1} \tag{24}$$

where

$$K_*^2 = (\omega - uk_1)^2/v^2 + K^2 + \Delta^{-2}$$

ν and c_ν are dimensionless constants, and other quantities will be discussed presently. For convenience, we now use k_1, k_3 to denote the flow-related components previously denoted by $\tilde{k}_1$, $\tilde{k}_3$. In Eq. (24), the inverse dependence on the wavenumber variable K_* yields the usual sharp mean-convective peak at streamwise wavenumber $k_1 \simeq \omega/u$, by virtue of the first term in K_*^2 and the smallness of the dispersive velocity ratio v/u. In a reference frame moving streamwise at the effective mean convection speed u, the pressure spectral density has the same form except that the term $-uk_1$ in K_*^2 is absent; in this moving frame the spectrum, apart from the factor k_1^2, may be described as space-time isotropic with a turbulence-velocity scale v and a large-eddy scale Δ.

With regard to the factor k_1^2, the relation of pressure to its velocity-derivative sources in incompressible turbulent-boundary-layer flow indicates that such a factor would be expected from the mean-shear source term. The pure-turbulence source terms, on the other hand, would yield a more nearly isotropic factor like K^2. The factor k_1^2 leads to a frequency spectrum of point pressure proportional to ω^2 at moderately low frequencies where $v/u \lesssim \omega\Delta/u \lesssim 1$ [e.g., see Eq. (25)], whereas an isotropic factor instead yields one independent of frequency where $\omega\Delta/u \lesssim 1$. On the basis of the rise in the near-field pressure spectrum measured in jet-flow experiments such as that considered later, we accept the factor k_1^2 and interpret this as indicating dominance of the hydrodynamic pressure fluctuations in jet flow off an edge by the mean-shear source term.

For the exponent ν in the model spectrum (24), a value 7/3 is chosen mainly on the basis of comparison of the limiting high-frequency dependence $\omega^{-2\nu+2}$ for the radiated pressure spectrum with that measured, as will be shown presently. A value $\nu = 2$, we note, would yield a spectrum $P(\mathbf{K}, \omega)$ independent of the scale Δ at frequencies well above the convective large-eddy frequency u/Δ. Such independence conforms to the similarity character of measured wall-pressure fluctuations beneath a turbulent-boundary layer. With the scale Δ taken of the order of boundary-layer thickness and v about twice the wall-friction velocity, in fact, the given form with $\nu = 2$ yields the measured features of boundary-layer wall pressure fairly well.[10] On the other hand, for homogeneous isotropic turbulence in the inertial subrange, the spectral density of pressure in a uniformly moving frame has been predicted to have the form (24) with a factor $(k_1/K_*)^2$ removed and $\nu = 8/3$.[11] The intermediate value $\varphi = 7/3$ chosen here, together with the k_1^2 factor, is suggested independently of measured spectral slopes by supposing that the mean-shear source term predominates in the pressure near the edge in the subject sheared jet flow, but that the normal component of turbulent velocity entering this source term has the same similarity form as in the inertial subrange of isotropic turbulence. This supposition yields a pressure spectrum proportional to $\Delta^{-2/3}$ in agreement with the assumed form provided that $\nu = 7/3$.

We proceed to the evaluation of spectra of Sec. II by insertion of the explicit form (24). The frequency spectrum of pressure in the half plane $x > 0$, $y = 0$, i.e., of hydrodynamic pressure, can be obtained by integration of the lower form in Eq. (14):

$$\begin{aligned} P(\omega) = {} & 2\pi(2\nu-1)^{-1} c_\nu \rho^2 v^4 \omega^{-1} (\omega\Delta/u)^{-2(\nu-2)} \\ & \times [1 + (\omega\Delta/u)^{-2}]^{-\nu+1/2} \\ & \times \{1 + \mu^2 (2\nu-3)^{-1} [1 + (\omega\Delta/u)^{-2}]\} \end{aligned} \tag{25}$$

in which the factor { } will be approximated by unity where $\omega\Delta/u >> \mu (<< 1)$. Likewise, the spectrum of pressure radiated to the farfield, given by Eq. (16). is obtained by integration of Eq. (17)

$$\begin{aligned} P(\mathbf{r}, \omega) = {} & [\Gamma(\nu)/\pi^{1/2}\Gamma(\nu + 1/2)] c_\nu \rho^2 v^4 \omega^{-1} (\omega r/u)^{-1} \\ & \times (L/r)(u/c)(\omega\Delta/u)^{-2(\nu-2)} \\ & \times \sec\alpha \sin\theta \sin^2 \tfrac{1}{2}\phi [\sec^2\alpha + (\omega\Delta/u)^{-2}]^{-\nu} \end{aligned} \tag{26}$$

The speed and frequency dependences of $P(\omega)$ and $P(\mathbf{r}, \omega)$ in opposite limiting domains of $\omega\Delta/u$ are evident. The cross-coherence and phase between the farfield radiated pressure and the hydrodynamic pressure in the half-plane $x > 0$, $y = 0$ for $\alpha = 0$ given by Eq. (18) (with $\tilde{M} - M$) and Eqs. (22) and (23) are obtained by integration of Eq. (20)

$$C(x_0, \omega) = m_\nu (\omega L/u)^{-1/2} [1 + (\omega\Delta/u)^{-2}]^{-1/4} N_\nu(\xi) \tag{27}$$

where

$$\tau_m = c^{-1}(r - z_0 \cos\theta) - u^{-1} x_0 \tag{28}$$

$$\begin{aligned} m_\nu &\equiv [2\pi^{1/2}\Gamma(\nu)/\Gamma(\nu - 1/2)]^{1/2} \\ \xi &\equiv \mu |x_0| (\omega^2/u^2 + \Delta^{-2})^{1/2} \\ N_\nu(\xi) &\equiv \xi^\nu K_\nu(\xi)/2^{\nu-1}\Gamma(\nu) \end{aligned} \tag{29}$$

so that $N(1) = 1$], in which K_ν denotes the usual hyperbolic Bessel function.

On the other hand, on the rigid half-plane $x < 0$, $y = 0$, the spectrum of nearfield pressure given by Eq. (14) (upper form) and the cross-coherence C and phase τ_m referring to the rigid half-plane ($x_0 < 0$, $y = 0$) given by Eqs. (18, 19, 22, and 23) cannot be expressed in simple closed form but require numerical approximation of the integrals of Eqs. (14) and (19). The cross-coherence in this case, for $\omega\Delta/u >> 1$ (whence $\xi \to \mu\omega|x_0|/\mu = \mu\sigma$), has the form of Eq. (27) with $N_\nu(\xi)$ replaced by a certain other function $N_\nu(\mu\sigma, \sigma)$. This N_ν satisfies $N_\nu(0,0) = 1$ and, for $\mu\sigma >> 1$, approaches asymptotically $(4\pi)^{-1/2}\sigma^{-1/2}$; at intermediate values of σ, $N_\nu(\mu\sigma, \sigma)$ oscillates about the function $N_\nu(\mu\sigma)$ given by Eq. (29). For $\omega\Delta/u >> 1$, then, we have

$$C(x_0, \omega)\ (\omega L/u)^{1/2} = m_\nu N_\nu(\mu\sigma, \sigma) \tag{30}$$

a function of ω and x_0 only via $\omega|x_0|/u$; in particular, as $\omega|x_0|/u \to 0$, $C(x_0, \omega) \to m_\nu (\omega L/u)^{-1/2}$. The coefficient m_ν depends only weakly on ν, and $m_{7/3} = 2.12$. Rough expressions have been obtained for C and then $N_\nu(\mu\sigma, \sigma)$ by use of limiting forms for Erf ( ) in Eqs. (14) and (19).

IV. Application to a Jet-Flow Experiment

We turn to the jet-flow experiment by Scharton, Pinkel, and Wilby[9] illustrated in their Fig. 1, repeated here as Fig. 2. A jet stream for an orifice of diameter 1.75 in. with exit velocity 550 fps impinged on a flat surface and spilled off an edge. The frequency spectral density of pressure was measured by a sensor outside the flow and also by a sensor of diameter ⅛ in. flush-mounted in the surface beneath the flow at various distances upstream from the edge and by a probing sensor at various positions dowmstream. In addition, the maximum amplitude of the octave-band cross-correlation and the corresponding time-delay between the radiated-pressure sensor and the surface pressure sensor were measured at various positions and frequencies.

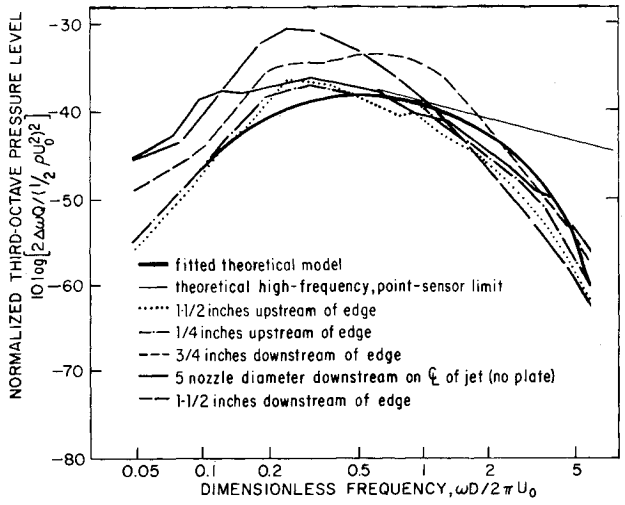

Fig. 3 Dimensionless third-octave pressure levels in plate beneath jet flow and downstream of edge. Measured results are those of Ref. 9. In the ordinate, Q is the pressure spectrum so normed that the mean square is

$$4\pi\int_0^\infty d(\omega/2\pi)Q(\omega), \text{ and } \Delta\omega/\omega = 0.23$$

The pressure autospectra measured by a sensor at various upstream and downstream positions are shown in Fig. 3 as third-octave levels vs fD/U_0. The variation of these spectra with position does not conform to the constancy downstream of the edge and oscillatory increase upstream predicted from a streamwise-homogeneous "incident" hydrodynamic pressure, but that assumption is necessarily crude. In any case, from the result (25) for the model hydrodynamic pressure spectrum, estimating the effective convective velocity u and choosing by adjustment the eddy-scale Δ and the multiplicative coefficient, we obtain the fitted result represented by the heavy curve in the figure. At the higher frequencies, the effect of area-averaging by the ⅛-in. sensor has been included by considering a factor $[2J_1(1.1\omega R/u)/(1.1\omega R/u)]^2$ to be applied to the point spectrum, as roughly appropriate for uniform averaging over an area of radius R. (The light straight line represents the high-frequency limiting form for a point sensor.) Specifically, it was assumed for the fitted curve that $2R = ⅛$ in., $u/U_0 = 0.4$ (e.g., $U/U_0 = 0.8$ and $u/U = 0.5$, where U is the maximum velocity in the streamwise and edgewise profiles at the edge) and‡

$$\nu = 7/3, \ \Delta/D = 0.267, \ c_\nu^{I/L} v/U_0 = 0.10 \qquad (31)$$

Given the character of the parameters Δ, c_ν, u, and v/u, the quoted values are of credible magnitude.

Returning for a moment to the dependence of the measured spectra of Fig. 3 on position and interpreting each hump as associated with a hydrodynamic pressure field with large-eddy scale reciprocally related to the frequency of the hump, we can suggest the following detailed but highly conjectural a posteriori account. Since the surface-pressure spectra at upstream positions differ little, the eddy-scale Δ that determines the frequency of the hump is independent of position (over the subject range) and presumably determined mainly by the nozzle diameter. The measured spectrum ¾ in. downstream of the edge lies somewhat higher and displays a second, more pronounced hump at higher frequency. It is suggested to regard this as due to independent addition of a component in the downstream pressure spectrum with a smaller scale (about half as large) that is characteristic of eddies generated at the edge and proportional to distance downstream. At the greater distance 1.5 in. downstream, this second scale, being twice as large, is then about the same as the (nozzle-related) scale of the first component of the pressure spectrum. Hence, the two

‡$c_{7/3}$ in Eq. (31) corresponds to $P(\omega)$ in Eq. (25) normed like $Q(\omega)$ in Fig. 3.

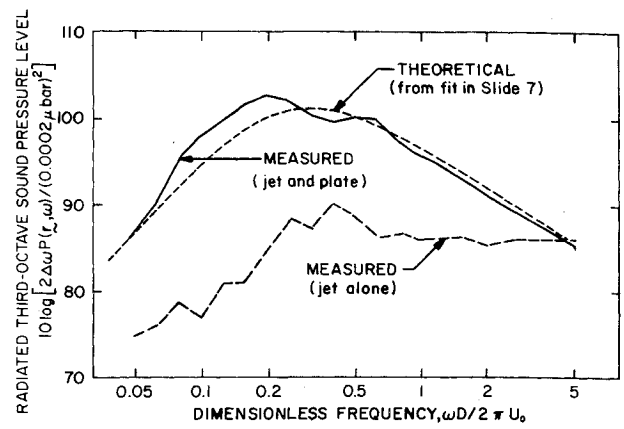

Fig. 4 Third-octave levels of sound radiated by jet flow. Measured results with and without plate edge are those of Ref. 9 for a microphone outside the flow on the flow side (Fig. 2).

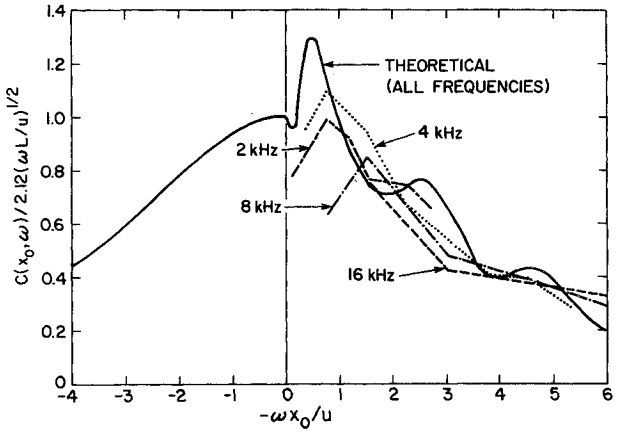

Fig. 5 Normalized cross-coherence of radiated sound and surface pressure at distance $-x_0$ forward of edge. Measured results are those of Ref. 9 for maximum cross-correlation in octave bands.

humps coincide in frequency and yield the single higher hump seen in the measured spectrum at this position. In the spectrum in Fig. 3 measured at 5 nozzle diameters downstream on the jet axis with plate absent, this spectrum increment attributed to eddy generation at the trailing edge is absent, and the peak strongly resembles that of the upstream spectra with plate present. A secondary hump appears, however, at a lower frequency corresponding to a scale about three times that of the primary hump; perhaps this is associated with a second large-eddy scale which in this case with no plate is proportional to distance downstream from the nozzle.

Proceeding to the radiated pressure, in Fig. 4 the third-octave spectrum measured at the position of the sensor removed from the flow is compared with the result computed from the model by Eq. (26) with $\alpha = 0$, $\theta = \pi/2$, $\phi = \pi/2$. We recall that the exponent ν was chosen in part to yield the correct slope at high frequencies, i.e., so that $\omega P(r,\omega) \propto \omega^{-5/3}$. In absolute level as well as shape, over the entire frequency range, the computed spectrum agrees with the measured one at least as well as did the fitted surface pressure spectrum shown in the preceding slide.

The measured maximum cross-correlation in octave bands between radiated sound and surface pressure at upstream (and a few downstream) locations was given for various frequencies in Ref. 9, Fig. 15. This quantity may be identified with an octave-band average of the cross-coherence C as defined in Eq. (21) and previously discussed. The measured normalized cross-correlations $C(x_0,\omega)\ (\omega L/u)^{1/2}/m_\nu$ are shown in Fig. 5 with L taken to have its estimated value $L = 2D = 3.5$ in. and $u/U_0 = 0.4$, $U_0 = 550$ fps, $m_\nu = m_{7/3} = 2.12$. Since $\omega\Delta/u >> 1$ for the frequencies of measurement, this normalized cross-

coherence, by Eq. (30), would be expected to be a universal function of $\omega|x_0|/u$ independent of frequency. The measured curves are seen to exhibit a fair degree of coalescence when scaled in this way. Equation (30) further expresses the predicted universal function as $N_\nu(\mu\sigma,\sigma)$. A rough evaluation of this function was performed for $\nu=7/3$ and $\mu=0.18$, the latter value being chosen as reasonable on the basis of application to turbulent boundary-layer wall pressure of a model similar to Eq. (24), and the result is also shown in Fig. 5. Its resemblance to the measured normalized cross-correlations may be considered satisfactory, especially since its apparently excessive oscillations would be reduced by performing the octave-average appropriate to the measurements. The predicted curve is given in Fig. 5 also for downstream points ($x_0>0$) (for which the diffracted wave vanishes), as obtained from Eq. (29), but the measured cross-correlations for downstream locations are omitted on account of their experimental variability.

The measured time delays for maximum correlation can be approximately identified with the delay τ_m in the cross-spectral phase defined in Eq. (21). It is stated in Ref. 9 that the measured delays were indistinguishable from the expected acoustic propagation time ($\simeq r/c$) between the two sensors. The predicted time referring to upstream locations oscillates about the result $r/c+(-x_0)/u(x_0<0)$ that would be given by supposing that the downstream form Eq. (28) applies. The latter result, for $u/U_0=0.4$, is greater than r/c by a maximum (at $-x_0=1.75$ in.) of 75%; re-examination of the measured data would be required to permit an adequate quantitative comparison.

V. Conclusion

The treatment of edge radiation by turbulent flow in terms of an assumed wavevector-frequency spectrum of hydrodynamic pressure, together with the proposed model form for this spectrum, thus yields results for radiated pressure and its cross-coherence with pressure near the edge that conform substantially with results of a jet-flow experiment. The comparison provides a measure of validation of the basic method and of the characterization of hydrodynamic pressure. The results supply a basis for estimating edge-radiated noise and may guide experimental investigations of other flow configurations.

We conclude by noting a nontrivial aspect of extension of the treatment from one-sided to two-sided flow. In two-sided flow, the pressure difference p_+-p_- across the surface enters as seen in Eq. (3), but its amplitude depends on the correlation of the oppositely incident evanescent waves, the determination or modeling of which has not been addressed. If the incident pressures were perfectly correlated but of opposite sign, for example, the total pressure on the extension half-plane (S_+) would vanish, and in the upstream pressure-doubling limit the total pressure on opposite sides of the rigid surface would be, respectively, ± 2 times the incident pressure on one side; the radiated pressure level in such case would be 6 db above that associated with incidence from one side only. In case of no correlation, the increase would instead be 3 db. But if the incident pressures were perfectly correlated and of the same sign, the pressure difference across the rigid half-plane would vanish and hence also the edge-radiated pressure. In this artificial example, the pressure on the extension half-plane would be twice either incident one, and the total pressure field everywhere the same as if this half-plane were also rigid. In reality, the correlation between pressures on opposite sides of a rigid surface in two-sided flow presumably depends in some way on distance from the edge, introducing streamwise statistical inhomogeneity in a more essential way than in the instance of one-sided flow. To guide the requisite modeling, it appears desirable, as suggested by Chandiramani,[2] to conduct experiments with two-sided flow configurations in which the spectrum of the pressure-difference, i.e., the lift, field is measured and also its cross-spectrum with radiated pressure and the cross-spectrum of pressures on opposite sides.

References

[1] Chase, D.M., "Sound Radiated by Turbulent Flow off a Rigid Half-Plane as Obtained from a Wavevector Spectrum of Hydrodynamic Pressure," *Journal of the Acoustical Society of America,* Vol. 52, Sept. 1972, pp. 1011-1023.

[2] Chandiramani, K.L., "Diffraction of Evanescent Waves, with Applications to Aerodynamically Scattered Sound and Radiation from Unbaffled Plates," *Journal of the Acoustical Society of America,* Vol. 55, 1974, pp. 19-29.

[3] Ffowcs-Williams, J.E. and Hall, L.H., "Aerodynamic Sound Generation by Turbulent Flow in the Vicinity of a Scattering Half Plane" *Journal of Fluid Mechanics,* Vol. 40, 1970, pp. 657-670.

[4] Powell, A., "Aerodynamic Noise and the Plane Boundary," *Journal of the Acoustical Society of America,* Vol. 32, 1960, pp. 982-990.

[5] Crow, S.E., "Aerodynamic Sound Emission as a Singular Perturbation Problem," *Studies in Applied Mathematics,* Vol. 49, 1970, pp. 21-44.

[6] Tam, C.K.W., "Discrete Tones of Isolated Airfoils," *Journal of the Acoustical Society of America,* Vol. 55, 1974, pp. 1173-1177.

[7] McKinzie, D.J., Jr. and Burns, R.J., *Journal of the Acoustical Society of America,* Vol. 55, 1974, pp. 572-573(A).

[8] Hayden, R.E., "Noise from Flow Interaction with Rigid Surfaces: A Review of Current Status of Prediction Techniques," CR-2126, 1972, NASA (also designated Bolt Beranek and Newman Inc., Rept. 2276).

[9] Scharton, T., Pinkel, B., and Wilby, J., "A Study of Trailing Edge Blowing as a Means of Reducing Noise Generated by the Interaction of Flow with a Surface," Rept. 2593, Sept. 1973, Bolt Beranek and Newman Inc., Cambridge, Mass.

[10] Chase, D.M., "Wavevector/Frequency Spectrum of Turbulent-Boundary Layer Pressure," *Proceedings of the 1971 Symposium on Turbulence in Liquids, National Science Foundation and Dept. of Chemical Engineers,* Univ. of Missouri-Rolla, 1972, pp. 94-104.

[11] Chase, D.M., "Space-Time Correlations of Velocity and Pressure and the Role of Convection for Homogeneous Turbulence in the Universal Range," *Acustica,* Vol. 22, 1969/70, pp. 303-320.